Climate Dynamics
https://doi.org/10.1007/s00382-018-4446-2

Rainfall from tropical cyclones: high-resolution simulations and seasonal forecasts

Wei Zhang[1] · Gabriele Villarini[1] · Gabriel A. Vecchi[2,3] · Hiroyuki Murakami[4,5]

Received: 4 May 2018 / Accepted: 10 September 2018

Abstract
This study examines the performance of the Geophysical Fluid Dynamics Laboratory Forecast-Oriented Low Ocean Resolution version of CM2.5 (FLOR; ~ 50-km mesh) and high-resolution FLOR (HiFLOR; ~ 25-km mesh) in reproducing the climatology and interannual variability in rainfall associated with tropical cyclones (TCs) in both sea surface temperature (SST)-nudging and seasonal-forecast experiments. Overall, HiFLOR outperforms FLOR in capturing the observed climatology of TC rainfall, particularly in East Asia, North America and Australia. In general, both FLOR and HiFLOR underestimate the observed TC rainfall in the coastal regions along the Bay of Bengal, connected to their failure to accurately simulate the bimodal structure of the TC genesis seasonality. A crucial factor in capturing the climatology of TC rainfall by the models is the simulation of the climatology of spatial TC density. Overall, while HiFLOR leads to a better characterization of the areas affected by TC rainfall, the SST-nudging and seasonal-forecast experiments with both models show limited skill in reproducing the year-to-year variation in TC rainfall. Ensemble-based estimates from these models indicate low potential skill for year-to-year variations in TC rainfall, yet the models show lower skill than this. Therefore, the low skill for interannual TC rainfall in these models reflects both a fundamental limit on predictability/reproducibility of seasonal TC rainfall as well as shortcomings in the models.

1 Introduction

Rainfall associated with tropical cyclones (TCs) plays an important role in terms of rainfall extremes and climatology in both the tropics and the mid-latitudes (Rogers et al. 2006; Jiang and Zipser 2010; Khouakhi et al. 2017), and it has also been found to help in reducing the duration of droughts (Maxwell et al. 2012; Kam et al. 2013). TC rainfall and associated flooding have been responsible for significant societal and economic impacts (Rappaport 2014; Czajkowski et al. 2017; Peterson et al. 2013), with Hurricane Harvey being one of the latest examples (Emanuel 2017; Risser and Wehner 2017; van Oldenborgh et al. 2017). Therefore, a realistic simulation and characterization of TC rainfall in climate models could provide a tool for understanding and predicting TC-induced flooding, and contribute to improving our preparedness, mitigation and management of TC-related hazards.

Previous studies used observations to investigate the contribution of TC rainfall to the total precipitation at regional (Jiang and Zipser 2010; Barlow 2011; Dare et al. 2012; Lavender and Abbs 2013; Prat and Nelson 2013; Chen and Fu 2015; Gu et al. 2017; Gaona et al. 2018) and global scales (Jiang and Zipser 2010; Jiang et al. 2011; Kamahori 2012; Skok et al. 2013; Khouakhi et al. 2017). For example, the rainfall associated with these storms contributes to around 50% of the total precipitation over a majority of tropical ocean basins (Jiang and Zipser 2010) while around 4% of the total rainfall in the tropical North Atlantic is related to these

Electronic supplementary material The online version of this article (https://doi.org/10.1007/s00382-018-4446-2) contains supplementary material, which is available to authorized users.

✉ Wei Zhang
wei-zhang-3@uiowa.edu

[1] IIHR-Hydroscience and Engineering, The University of Iowa, Iowa City, IA, USA

[2] Department of Geosciences, Princeton University, Princeton, NJ, USA

[3] Princeton Environmental Institute, Princeton University, Princeton, NJ, USA

[4] National Oceanic and Atmospheric Administration/Geophysical Fluid Dynamics Laboratory, Princeton, NJ, USA

[5] Atmospheric and Oceanic Sciences Program, Princeton University, Princeton, NJ, USA

Published online: 14 September 2018

storms. TC rainfall accounts for up to 54% of total rainfall in the northern Philippines (Bagtasa 2017), with a maximum of 30% northeast of Puerto Rico (Rodgers et al. 2001). TC rainfall is important not only in terms of seasonal or annual contributions, but also in terms of extremes, with analyses performed at the regional (Larson et al. 2005; Shepherd et al. 2007; Lau et al. 2008; Knight and Davis 2009; Barlow 2011; Chen et al. 2013; Villarini and Denniston 2016) and global scales (Prat and Nelson 2016). Recently, Khouakhi et al. (2017) provided a comprehensive overview of the role that TCs play in terms of overall and extreme rainfall over land at the global scale, highlighting regions that are more susceptible to this hazard.

In addition to analyses using observational data, modeling studies have used general circulation models (GCMs) to evaluate the responses of TC rainfall to increased CO_2 (Scoccimarro et al. 2014, 2017; Villarini et al. 2014). The rate of TC rainfall is expected to increase with respect to anthropogenic forcing (Langousis and Veneziano 2009; Knutson et al. 2010; Villarini et al. 2014; Lin et al. 2015; Scoccimarro et al. 2017); Using idealized experiments, a doubling of CO_2 without increasing sea surface temperature results in a reduction in TC rainfall while a uniform increase of 2 K in sea surface temperature (SST) (with or without CO_2 doubling) leads to an increase in TC rainfall (Villarini et al. 2014). In contrast to the rate, TC rainfall area is modulated by relative SST, which results in small globally-averaged projected to changes, though there can be substantial redistributions in space (Lin et al. 2015). The capability of GCMs in reproducing TC rainfall has been evaluated in different studies, including the Geophysical Fluid Dynamics Laboratory (GFDL) HiRAM (Lin et al. 2015) and the Centro Euro-Mediterrraneo sui Cambiamenti Climatici (CMCC) climate model (Villarini et al. 2014; Scoccimarro et al. 2017); using the Cloud-Resolving Storm Simulator (CReSS) of Nagoya University, the TC rainfall in two landfalling TCs was found to increase by about 5–25% and with a tendency for the increases to be larger toward higher rain rates (Wang et al. 2014). A study focused on the North Atlantic with the GFDL-FLOR model found that shifts to the latitude of extratropical transition could lead to increases in rainfall from landfalling TCs along the Northeast of the United States (Liu et al. 2018).

Although major advancements have been made on the extent to which TC rainfall accounts for total rainfall at global and regional scales and on its association with extreme precipitation events, little attention has been paid to the seasonal forecast of this quantity. This is partly because the current generation of climate models are not very skillful at making seasonal forecasting of TC rainfall due to the complexities associated with correctly forecasting TC genesis, track, TC–land interactions, and the physical processes underlying the TC rainfall distributions. To the best of our knowledge, the only research on seasonal forecast of TC rainfall was attempted for Texas at the annual scale using multiple linear regression models (Zhu et al. 2013).

Among the existing models, the GFDL Forecast-Oriented Low Ocean Resolution version of CM2.5 (FLOR) has shown reasonable skill at representing the observed TC genesis, tracks and intensity (Vecchi et al. 2014; Zhang et al. 2016a, 2018; Murakami et al. 2017). Overall, the high-resolution version of FLOR (HiFLOR) was shown to further improve the simulation of TCs, extreme precipitation, climatology of the North American monsoon in the Gulf of California and the seasonal forecast of major hurricanes (Murakami et al. 2015, 2016; Pascale et al. 2016, 2017; van der Wiel et al. 2016; Zhang et al. 2016b). Despite the promising capability of FLOR and HiFLOR in reproducing the TC characteristics, little is known about their skill in reproducing TC rainfall using SST nudged to the observed estimates, and in forecasting the seasonal TC rainfall. Therefore, the goals of this study are to quantify the capabilities of FLOR and HiFLOR in reproducing the TC rainfall at the global scale, as well as the skill in forecasting this quantity at the seasonal scale.

The remainder of the paper is organized as follows. Section 2 describes the data and the methodology, followed by Sect. 3 where we present the results related to the climatology of TC rainfall, its interannual variability and response to El Niño/La Niña conditions. Section 4 summarizes the main results and concludes the paper.

2 Data and methodology

2.1 Data

The observed TC data are obtained from the International Best Track Archive for Climate Stewardship (IBTrACS; v03r10) with longitude, latitude, date and TC intensity for all recorded storms (Knapp et al. 2010). In terms of observed precipitation, we use the Multi-Source Weighted-Ensemble Precipitation (MSWEP) V2, which is based on a combination of rain gauge measurements, satellite products and reanalysis data (Beck et al. 2017a, b). Because MSWEP V2 is available at the 0.1-degree spatial and 3-h temporal resolution, we remap it to 0.25×0.25 degree spatial resolution and aggregate it to 6-h time scale to match the HiFLOR outputs. TC rainfall is defined as the rainfall within a 500-km radius of each TC center because this radius can account for the rainfall located from the inner core of the TC and the adjacent rainbands (Dare et al. 2012), and we only consider precipitation over land.

2.2 Climate models and experiments

The SST-nudging and seasonal-forecast experiments are performed with FLOR and HiFLOR. FLOR is developed by combing the oceanic and ice components of GFDL Coupled Model version 2.1 (CM2.1) (Delworth et al. 2006), with some modifications to the numerics and physical parameterizations in the ocean component from CM2.1, and the atmosphere and land components of CM2.5 (Delworth et al. 2012). The atmosphere and land components of TC-permitting FLOR have a spatial resolution of approximately ~ 50 km. The initial conditions of the ocean and sea–ice components are obtained from the GFDL's ensemble coupled data assimilation system (ECDA) (Zhang and Rosati 2010), while those for the atmospheric and land components are from the atmosphere-only simulations with FLOR by prescribing SST (Vecchi et al. 2014). HiFLOR is developed based on FLOR by increasing the horizontal resolution from ~ 50 to ~ 25 km, with the same sub-grid physics and with ~ 100-km mesh sea ice and ocean component (Murakami et al. 2015, 2016). The seasonal forecasts for the atmosphere and land components of HiFLOR are initialized with an arbitrary year from a control simulation in which anthropogenic forcing is fixed at the 1990 level (Murakami et al. 2015). By doing this, the forecasts of HiFLOR are constructed so that the predictability comes merely from the conditions of ocean and sea–ice. We evaluate the seasonal forecasts of TC rainfall with FLOR and HiFLOR for target months July–November (JASON) initialized in July and for target months January–May (JFMAM) initialized in January. TCs are tracked using the algorithm by Harris et al. (2016).

The SST-nudging experiments include six-member experiments for the period 1980–2015, in which the SST and sea surface salinity are nudged to the observed estimates at 5-day and 10-day scales using FLOR and HiFLOR. The SST-nudging experiments are used to assess whether the forcing of the observed SST can reproduce the observed TC rainfall. Both FLOR and HiFLOR have six-member SST-nudging experiments: three members for 5-day and 10-day nudging time scales, respectively. However, Murakami et al. (2015) discuss that there is no significant difference between 5-day and 10-day nudging time scales in terms of TC statistics such as interannual variation of TC frequency. Therefore, we consider these members as a same ensemble in this study. In addition to the SST-nudging experiments, we also use 12-member seasonal forecast experiments with both FLOR and HiFLOR.

Here we examine TC rainfall and its proportion to total precipitation using observations and climate model simulations. We evaluate the skill of the two GFDL models in representing the year-to-year variations in TC rainfall in terms of the mean square error (MSE) skill score SS_{MSE} (Hashino et al. 2007), which has been used in previous studies (Slater et al. 2017; Zhang et al. 2017):

$$SS_{MSE} = 1 - \frac{MSE}{\sigma_o^2} \tag{1}$$

where σ_o represents the standard deviation of the observed TC rainfall. A perfect forecast/SST nudging run has an SS_{MSE} value of 1 and the performance drops when the values are smaller than 1. An SS_{MSE} value of 0 suggests that the forecast accuracy is the same as the performance using climatology as the forecast/SST nudging. In addition, a negative skill score indicates that the accuracy is even worse than the forecast/SST-nudging run using climatology. The value of SS_{MSE} can be decomposed into three parts (Murphy and Winkler 1992):

$$SS_{MSE} = \rho_{fo}^2 - \left[\rho_{fo} - \frac{\sigma_f}{\sigma_o}\right]^2 - \left[\frac{\mu_f - \mu_o}{\sigma_o}\right]^2 \tag{2}$$

where ρ_{fo} denotes the correlation coefficient between observations and GCM outputs, and ρ_{fo}^2 represents the potential skill (coefficient of determination), which is the skill that can be reached in the absence of biases; σ_f and σ_o denote the standard deviation of forecasted/simulated and observed quantities, respectively; μ_f and μ_o represent the mean of forecasted/simulated and observed TC raiall, respectively. The second term $\left[\rho_{fo} - \frac{\sigma_f}{\sigma_o}\right]^2$ denotes the conditional bias known as the slope reliability (SREL). The third term $\left[\frac{\mu_f - \mu_o}{\sigma_o}\right]^2$ is the unconditional bias (i.e., standardized mean error (SME)). The decomposition of the forecast skill score (SS_{MSE}) can quantitatively diagnose the skill of the forecast, and identify potential biases (e.g., conditional and unconditional biases). If the potential skill is low, predictability is low even if the biases are corrected.

Because the TC rainfall and its proportions with respect to the total seasonal rainfall have zero values in some grids for the period 1980–2015 (i.e., sample size equal to 36), we exclude the grids with more than 20 out of 36 zero values when calculating the skill. We also mask out the regions with average observed TC density (binned into $1° \times 1°$ spatial grids) smaller than 2 during JASON, and those with average observed TC density smaller than 1 during JFMAM when calculating the skill score SS_{MSE} and its decompositions.

3 Results

3.1 Climatology of TC rainfall and its fractional contribution

We first evaluate whether the SST-nudging experiments can reproduce the observed climatology of TC rainfall during JASON for the period 1980–2015. Overall, the observed climatology of TC rainfall in East and South Asia has a larger magnitude than that in North America (Fig. 1, top panels). This is supported by a higher TC density in East and South Asia than in North America, as shown in observations and climate models (Figure S1). In particular, the Philippines, southern and eastern China, Vietnam, southern Japan, northeastern Indian and Myanmar receive an average of more than 100 mm of rainfall from TCs, with some regions receiving more than 120 mm. With a magnitude of ~ 60 mm, TC rainfall in the southeastern United States, the Caribbean regions, Mexico and Central America is much lower than what observed along the East Asian coastal regions (Fig. 1). HiFLOR (Fig. 1, middle panels) produces TC rainfall with magnitudes larger than the observations in South China, Thailand, Vietnam, Korea and South Japan, while it underestimates it in the Northeastern Indian coast and Myanmar, probably because

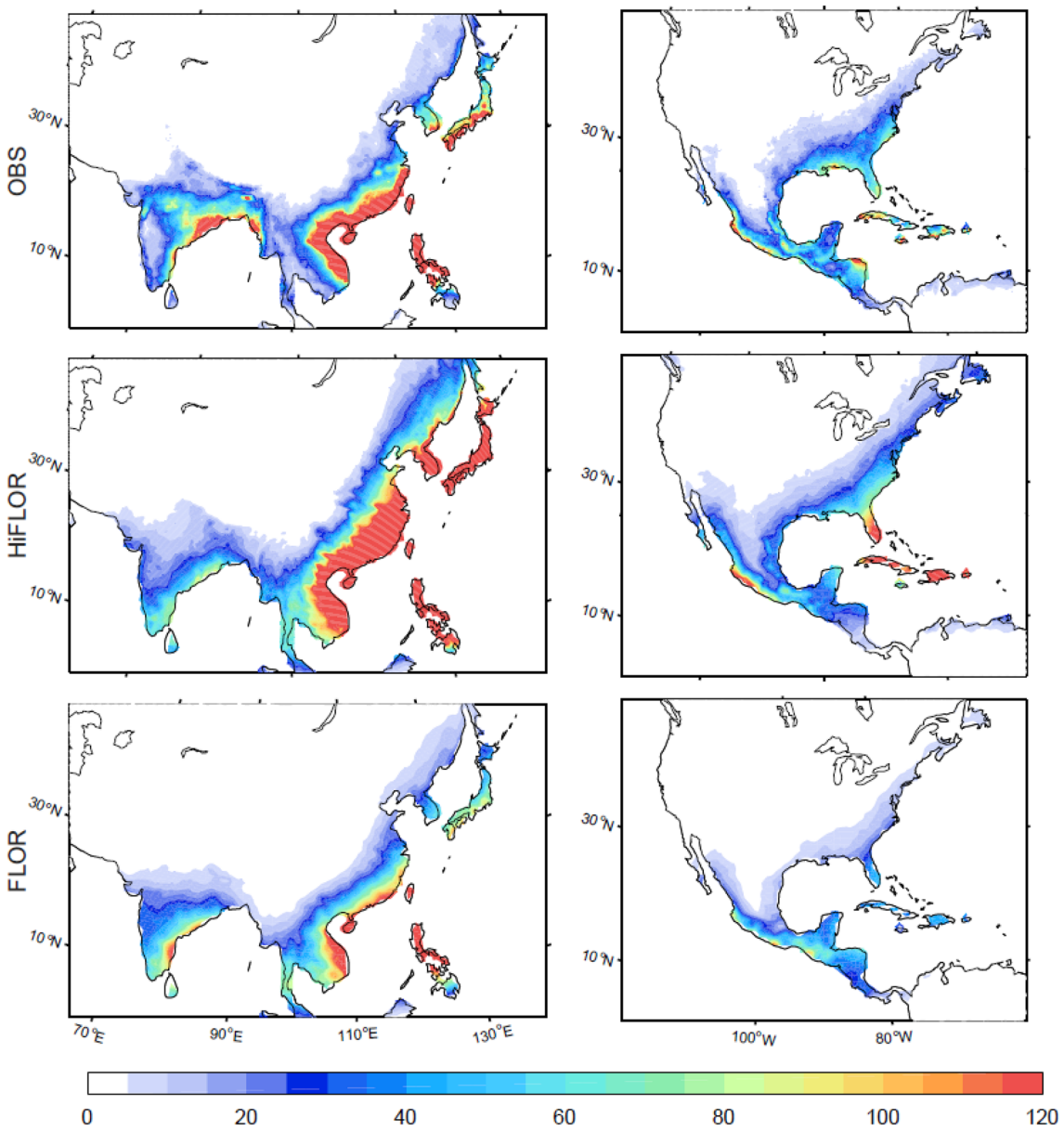

Fig. 1 Climatology of JASON TC rainfall (unit: mm) for the period 1980–2015 in (top) the observations, (middle) HiFLOR, and (bottom) FLOR

of a lower TC density than in the observations (Figure S1). HiFLOR also produces slightly higher TC rainfall than observations in North and Central America (Fig. 1, middle right panel), while FLOR produces much less TC rainfall in these regions (Fig. 1, bottom right panel). FLOR simulates less rainfall than the observations in Asia except the Eastern Indian coast where FLOR produces slightly more rainfall (Fig. 1, bottom left panel). FLOR simulates less than 100 mm of TC rainfall in a large portion of South China and Thailand, where the TC rainfall in observations is higher than 100 mm (Fig. 1, bottom left panel). Overall, HiFLOR captures the climatology of TC rainfall in Asia and North America reasonably well, while FLOR markedly underestimates it in almost all the Asian regions (except for the southeastern Indian coast) and North America (Fig. 1).

During JFMAM, the observed TC rainfall in Asia is lower than that during JASON, especially along the Northeastern Indian coast, South China, Korea and Japan (Fig. 2). There are high values of TC rainfall in the Myanmar coast during JFMAM, consistent with relatively high TC density in this region (Figure S2), associated with the bimodal structure of TC genesis seasonality in the Bay of Bengal (Li et al. 2013). In Australia, there are large values (in excess of 60 mm) of observed TC rainfall in the northern part (Fig. 2, top right panel), consistent with high TC density for the

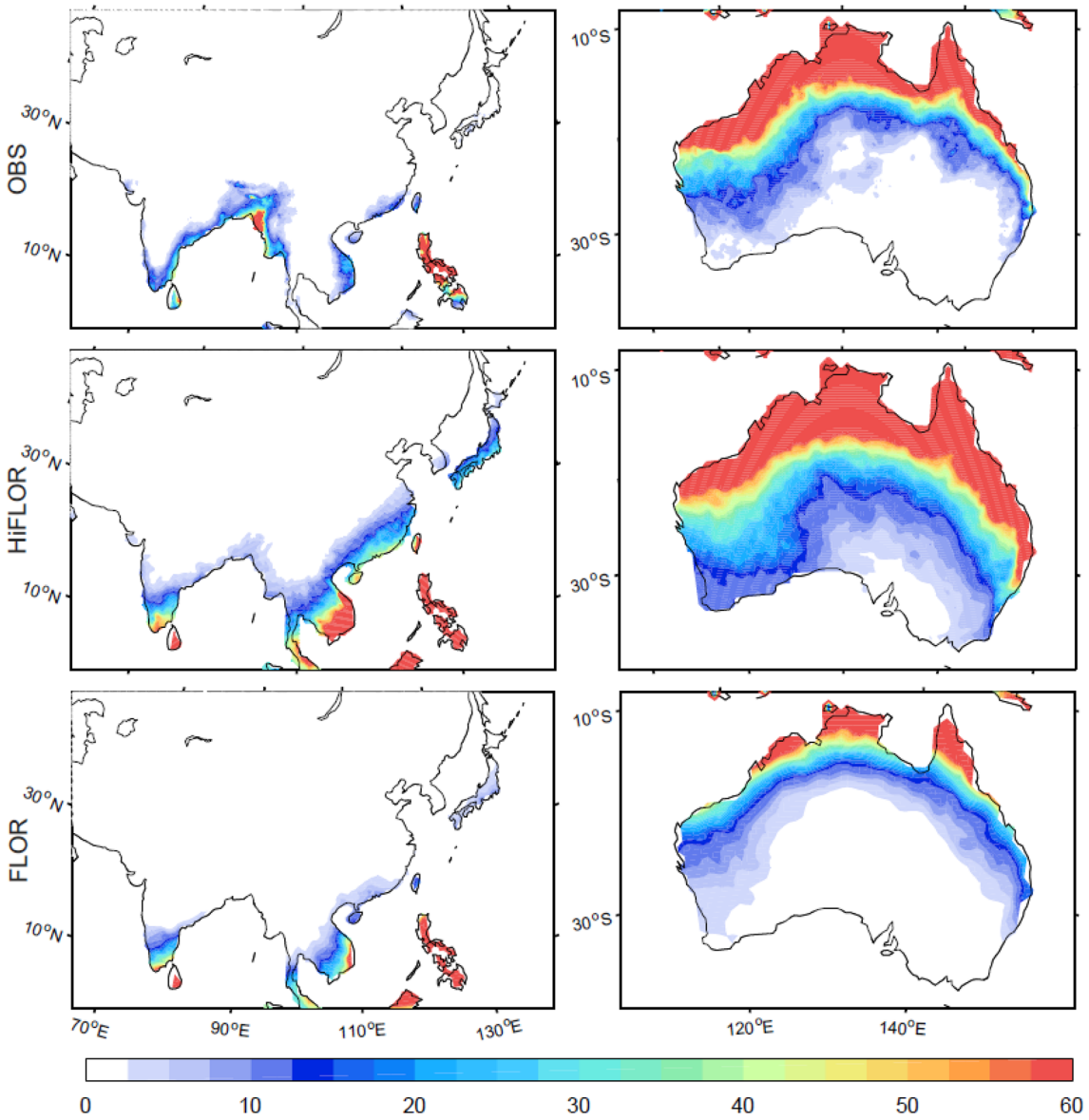

Fig. 2 Climatology of JFMAM TC rainfall (units: mm) for the period 1980–2015 in (top) the observations, (middle) HiFLOR, and (bottom) FLOR

region (Figure S2, top panel). HiFLOR reproduces well the observed TC rainfall in the Philippines, whereas there is an overestimation in southeastern China, Japan, Vietnam, Thailand and Southern India (Fig. 2, middle left panel). However, HiFLOR underestimates the TC rainfall in the Myanmar coast, probably because HiFLOR produces lower TC density in this region than in the observations (Figure S2, middle panel). In Australia, HiFLOR reproduces TC rainfall reasonably well in the northern part compared with the observations, albeit with slightly larger amounts in the southern part (Fig. 2, middle right panel). FLOR reproduces reasonably well the observed rainfall associated with TCs during JFMAM in Vietnam, the Philippines, South China, Korea and Japan but it also underestimates it in the Myanmar coast (Fig. 2, bottom right panel). FLOR clearly simulates lower TC rainfall values than in the observations in Australia during JFMAM, and this is particularly true in the northern part (Fig. 2, bottom right panel).

Overall, these results show that HiFLOR slightly overestimates the observed TC rainfall in Asia and North America during JASON, while FLOR markedly underestimates it. During JFMAM, HiFLOR produces excessive TC rainfall in South China, the Philippines, Vietnam, Thailand and southeastern India, while FLOR produces more realistic rainfall footprints. In the northern part of Australia, HiFLOR outperforms FLOR in reproducing the rainfall associated with TCs during JFMAM.

In addition to considering the total TC rainfall, we also consider its contribution to the total TC rainfall for a given season. During JASON, TC rainfall accounts for more than 25% of total precipitation in Southeast China and the Philippines, while the proportion slightly drops to around 20% in Vietnam, Japan and Korea, and to 10% in the coastal regions of East India and Bengal (Fig. 3, top left panel). Along the southeastern U.S. coast, TC rainfall accounts for ~12% of the total precipitation, while this percentage increases to 25% in Baja California (Fig. 3, top right panel). HiFLOR simulates the proportion of TC rainfall in East Asia similar to the observations, albeit with a larger magnitude in southeastern China, Korea and Japan (Fig. 3, middle left panel). Moreover, HiFLOR reproduces very well the observed portion of TC rainfall in North America during JASON (Fig. 3, middle right panel). FLOR greatly underestimates the proportion of TC rainfall in southeastern China, Vietnam, Philippines, Japan and Korea; however, FLOR appears to perform better than HiFLOR in simulating the proportion of TC rainfall along the southeastern Indian coast. FLOR markedly underestimates the proportion of TC rainfall in North America during JASON (Fig. 3, bottom right panel).

During JFMAM, the regions with relatively high fractional contributions of TC rainfall are located in the Philippines and the coastal regions in Bay of Bengal (Fig. 4, top left panel). HiFLOR performs better than FLOR in reproducing the observed TC rainfall proportions in those regions (Fig. 4, middle and bottom left panels). Specifically, HiFLOR slightly overestimates the proportion of TC rainfall in southeastern China and Vietnam and Pakistan, and underestimates it in northeastern Indian and the Myanmar coast (Fig. 4, middle left panel), similar to the results for the total amounts (Fig. 2, middle left panel). During JFMAM, there is a high TC rainfall contribution in the western part of Australia (> 25%) in the observations (Fig. 4, top-right panel), and HiFLOR reproduces it quite well (Fig. 2, middle right panel); however, FLOR underestimates the proportion of TC rainfall in Asia and in Australia (Fig. 4, bottom panels).

The climatology of observed TC rainfall during JASON is reasonably reproduced in the 12-member seasonal forecast experiments with HiFLOR in Asia and North America (Fig. 5, middle panels). In the coastal regions of the Bay of Bengal, the seasonal forecast experiments with HiFLOR tend to underestimate the climatology of observed TC rainfall during JASON, especially in Myanmar and eastern India. Overall, the seasonal forecast experiments with FLOR underestimate the rainfall associated with these storms during JASON, except for eastern India where the values are larger than observed (Fig. 5, bottom panels), consistent with the overestimation of the TC density by FLOR over this region (Figure S3). In North America, HiFLOR outperforms FLOR in forecasting the climatology of TC rainfall (Fig. 5, right-middle panel). The magnitude and regional patterns of this quantity are reasonably well forecasted with HiFLOR, while FLOR appreciably underestimates them in North America (Fig. 5).

During JFMAM, the climatology of TC rainfall in the observations is captured reasonably well in Asia with both FLOR and HiFLOR (Fig. 6), with the exception of Myanmar. Moreover, the seasonal forecast experiments with HiFLOR reproduce quite well the climatology of TC rainfall in Australia, while those with FLOR significantly underestimate it (Fig. 6, right panels). The performance of FLOR and HiFLOR in capturing TC rainfall in seasonal forecast experiments is consistent with the capability of the two models in simulating TC density during JASON and JFMAM (Figures S3-4).

The proportion of observed TC rainfall during JASON in East Asia bears strong resemblance to that with HiFLOR (Fig. 7, middle left panel), even though it underestimates it in the Bay of Bengal and the southeastern Indian coast. The seasonal forecast experiments with FLOR markedly underestimate the fractional contribution of TC rainfall in the coastal regions along the Bay of Bengal, but performs even better than HiFLOR over eastern India (Fig. 7, bottom left panel). In North America, the seasonal forecast experiments with HiFLOR outperform FLOR in reproducing the TC fractional contribution (Fig. 7, middle right panel), similar to the results for the total amounts (Fig. 5). During JFMAM,

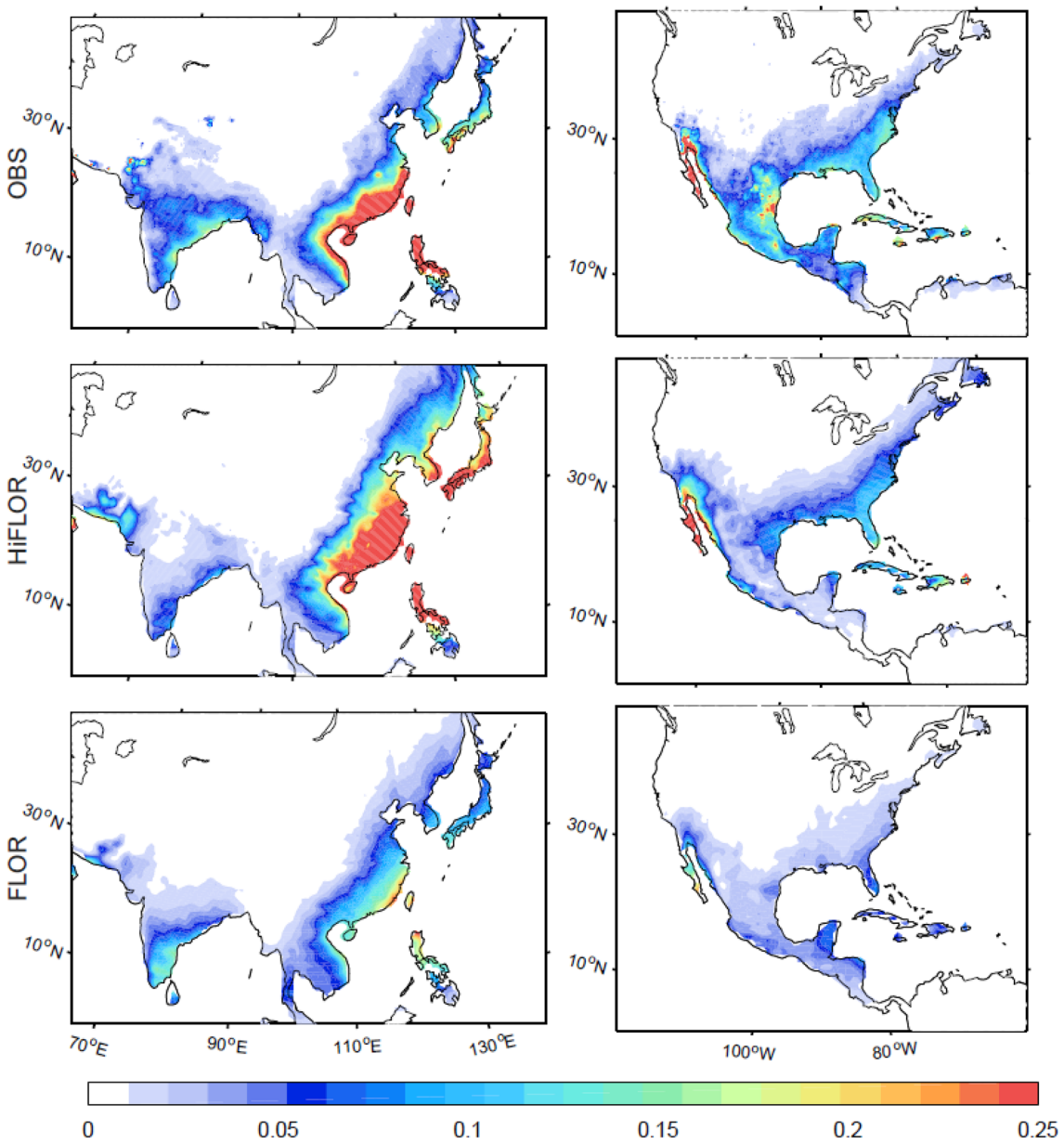

Fig. 3 Climatology of the proportion of JASON TC rainfall to total TC rainfall for the period 1980–2015 in (top) the observations, (middle) HiFLOR, and (bottom) FLOR

HiFLOR and FLOR produce much lower values of the fractional contributions in the Bay of Bengal and along the eastern Indian coast, and perform reasonably well in Vietnam and the Philippines (Fig. 8, left panels), consistent with the results for the TC density (Figure S4). HiFLOR performs much better than FLOR in reproducing the observed TC percentages in Australia during JFMAM, and this is particularly true in eastern Australia (Fig. 8, right panels).

These results have demonstrated the capability of FLOR and HiFLOR in reproducing the climatology of TC rainfall and its fractional contribution to the seasonal totals in the SST-nudging and seasonal forecast experiments. Overall, HiFLOR performs better than FLOR in capturing the climatological and regional structures of these quantities, suggesting that high-resolution simulations play an important role in a more accurate representation of TC rainfall.

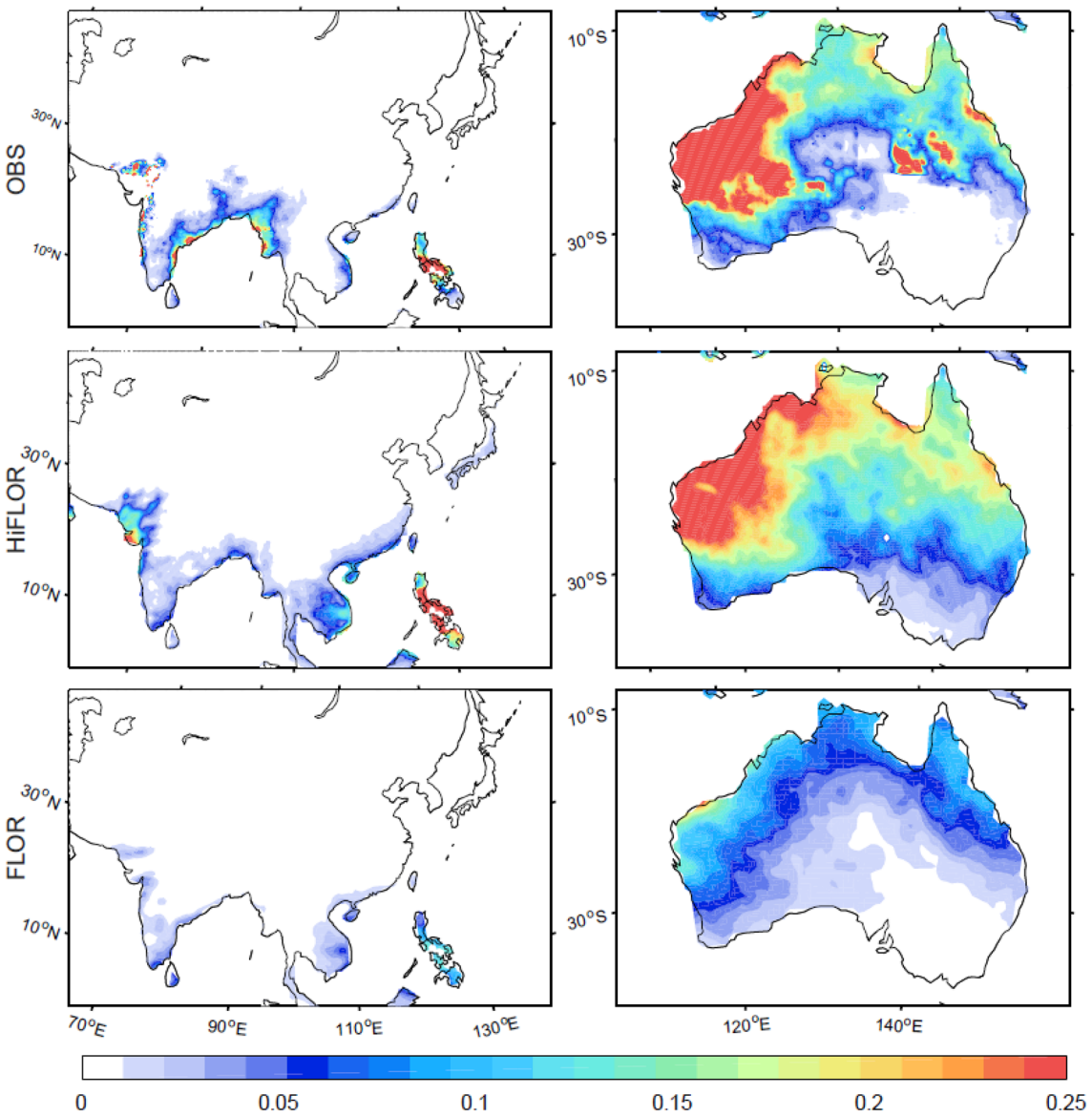

Fig. 4 Climatology of the proportion of JFMAM TC rainfall to total TC rainfall for the period 1980–2015 in (top) the observations, (mid) HiFLOR, and (bottom) FLOR

3.2 Year-to-year variation of TC rainfall and its fractional contribution

During JASON, the skill of the correlation coefficient between simulated TC rainfall in the SST-nudging experiments with FLOR and HiFLOR and observed TC rainfall is low in both Asia and North America, with HiFLOR and FLOR showing similar potential skill (Fig. 9). HiFLOR has larger conditional and unconditional biases than FLOR, particularly in southeast China, Japan and Korea (Fig. 9). The unconditional biases can be related to the differences in mean storm-specific rainfall (Figure S5, left panels); the storm-specific rainfall in HiFLOR is, on average, larger than in the observations, while FLOR produces less storm-specific rainfall than the observations during JASON (Figure S5, left panels). The skill scores for TC

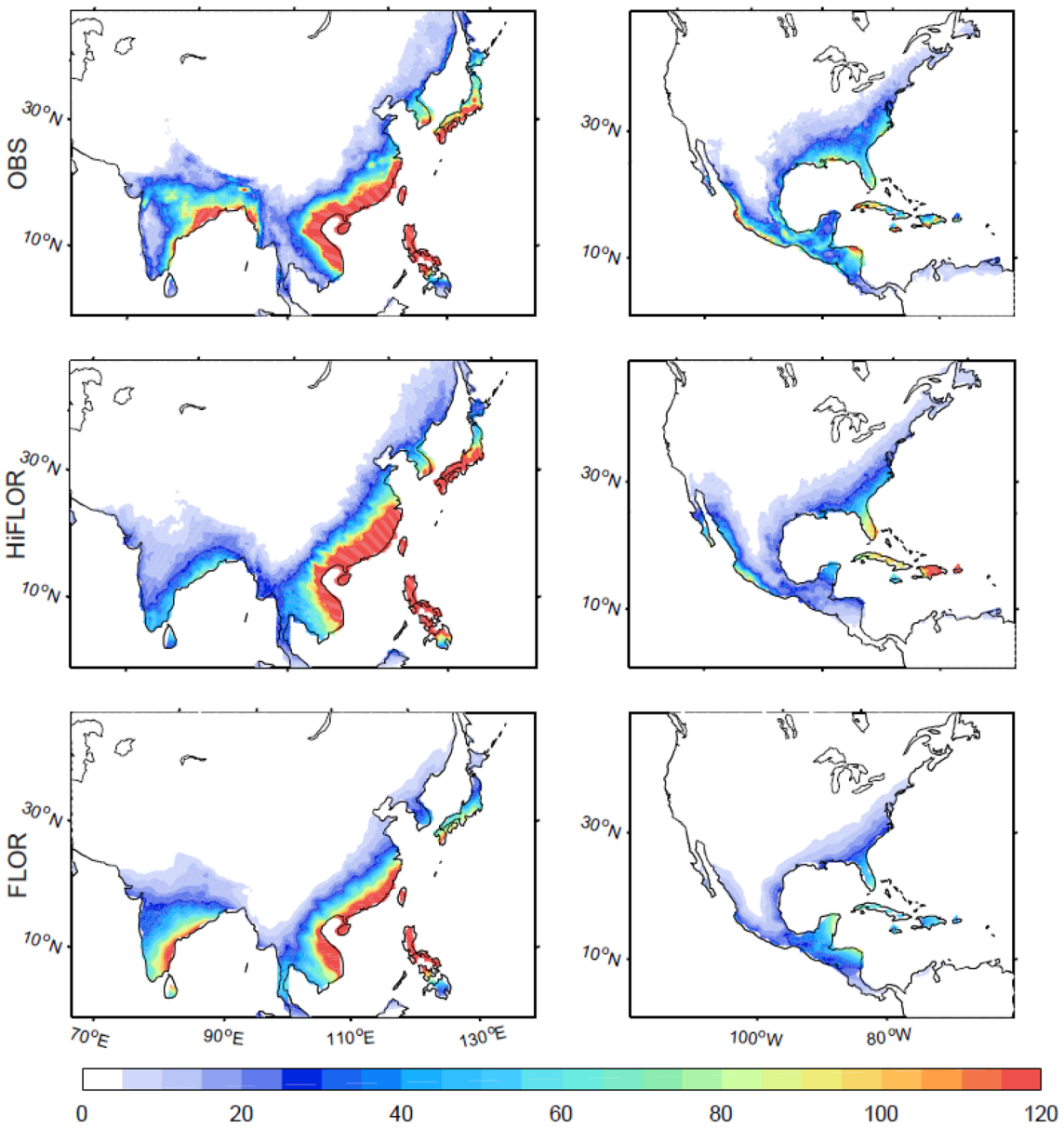

Fig. 5 (Top) observed climatology of JASON TC rainfall (unit: mm), and corresponding seasonal forecast initialized in July for the period 1980–2015 in (middle) HiFLOR and (bottom) FLOR

rainfall in FLOR and HiFLOR in Asia and North America are low, with some negative values indicating that the skill can be less than climatology (Fig. 9, bottom row).

During JFMAM, the vast majority of Asia is masked out because of the low TC density (figure not shown). Overall, the potential skill for TC rainfall is low in HiFLOR and FLOR, except for West Australia where FLOR shows encouraging values of the correlation coefficient (Fig. 10). HiFLOR produces larger unconditional and conditional biases in northern Australia (Fig. 10, left panels), while FLOR produces larger unconditional biases in East Australia (Fig. 10, right). The skill score in Australia is also negative in both HiFLOR and FLOR (Fig. 10). Consistent with that in JASON, the storm-specific rainfall in HiFLOR in JFMAM is much larger than in the observations, with FLOR producing less storm-specific rainfall than observed (Figure S5, right

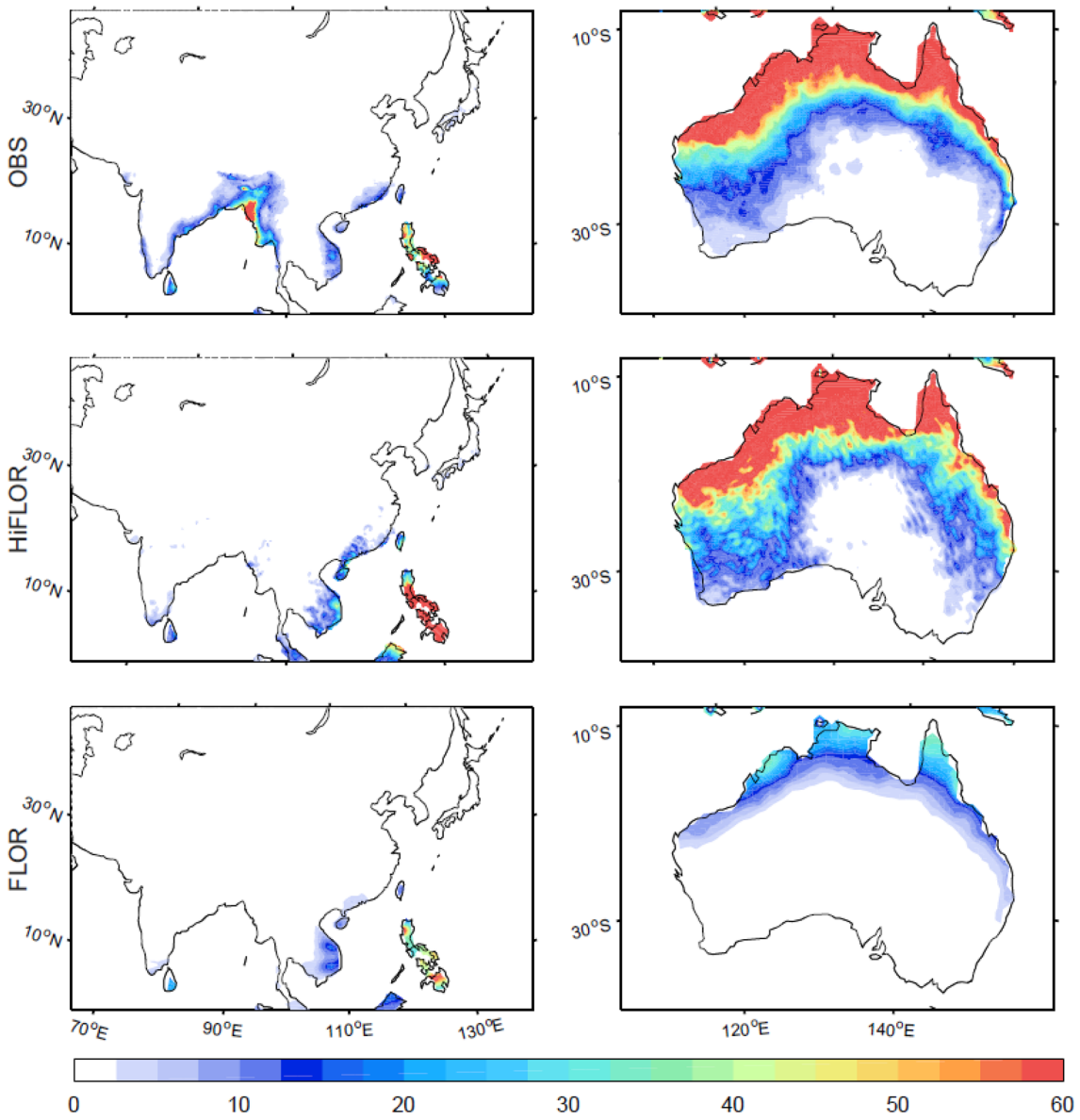

Fig. 6 (Top) observed climatology of JFMAM total TC rainfall (unit: mm), and seasonal forecasts of the climatology of JFMAM total TC rainfall initialized in January for the period 1980–2015 in (middle) HiFLOR and (bottom) FLOR

panels), suggesting that the mean biases in storm-specific rainfall with FLOR and HiFLOR can help diagnose the reasons for the limited forecast skill.

We examine the proportion of TC rainfall to total precipitation during JASON. Similar to the results for TC rainfall during JASON, both FLOR and HiFLOR exhibit limited potential skill in Asia and North America (Fig. 11). FLOR outperforms HiFLOR in southeastern China and some parts of Central America, while HiFLOR outperforms FLOR along the eastern Mexican coast. Both FLOR and HiFLOR produce large conditional and unconditional biases, which lead to very low (negative) skill score for the proportion of TC rainfall (Fig. 11).

During JFMAM, HiFLOR and FLOR exhibit potential skill for the proportion of TC rainfall in Australia (Fig. 12) which is similar to what observed in Fig. 10. HiFLOR has smaller conditional biases for the proportion of TC rainfall than FLOR in Northern Australia, while the opposite is true

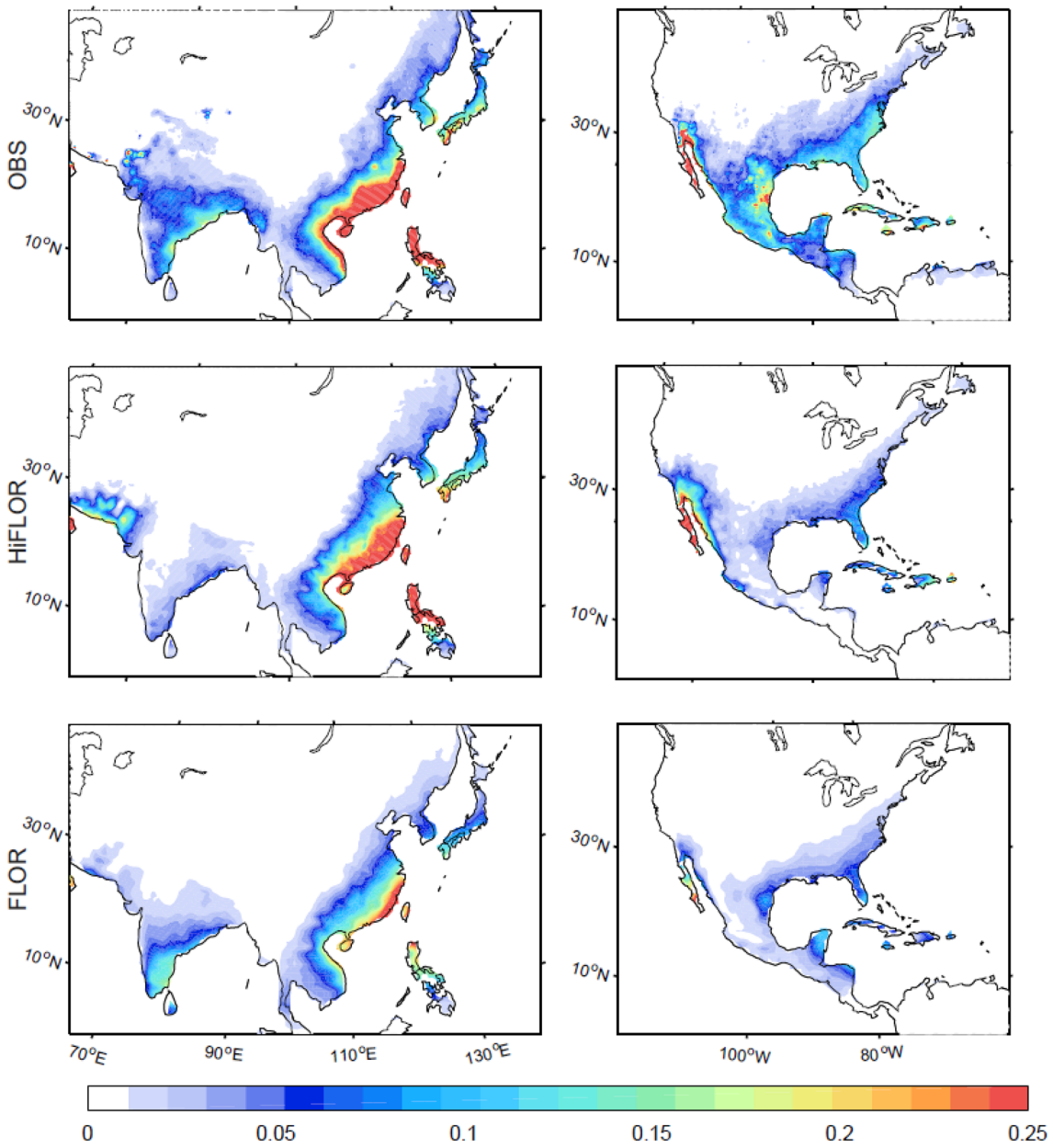

Fig. 7 (Top) observed climatology of the proportion of JASON TC rainfall, and seasonal forecasts of the climatology of this quantity initialized in July for the period 1980–2015 in (mid) HiFLOR and (bottom) FLOR

for unconditional biases (Fig. 12). Overall, the skill scores for the proportion of TC rainfall in Australia are similar (and negative) in both models (Fig. 12).

Given the lack of skill in reproducing the interannual variability in TC rainfall in the nudged experiments, we do not expect to see an improvement when we examine its predictability with several month lead times. This expectation in confirmed in Figures S6–9, where there is limited potential skill, large conditional and unconditional biases, and an overall negative skill score.

3.3 TC rainfall during El Niño and La Niña years

The analyses so far have focused on the examination of the capabilities of FLOR and HiFLOR in reproducing the TC rainfall footprint and its interannual variability. Here,

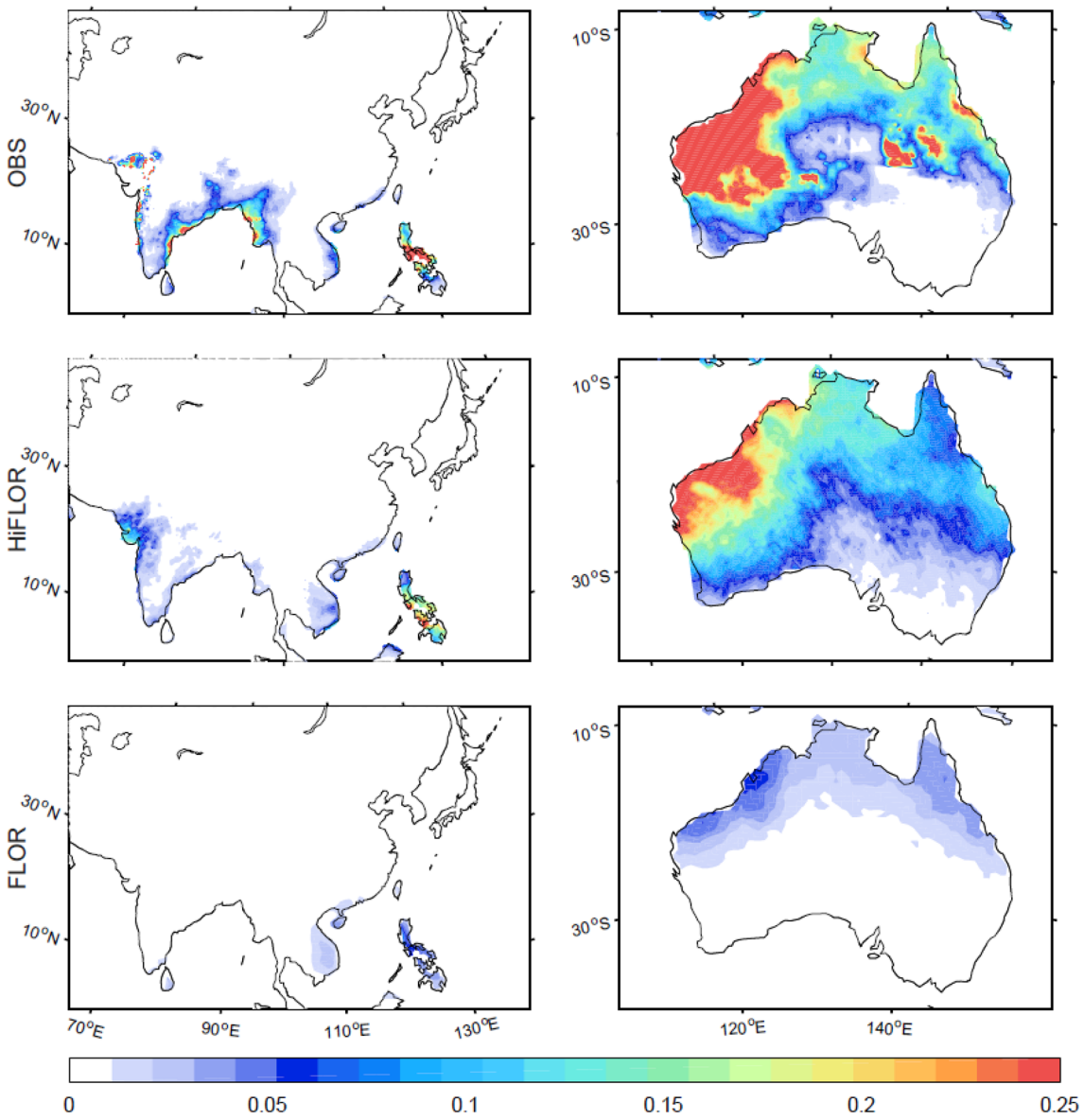

Fig. 8 (Top) observed climatology of the proportion of JFMAM TC rainfall, and seasonal forecasts of the climatology of this quantity initialized in January for the period 1980–2015 in (middle) HiFLOR and (bottom) FLOR

instead, we focus on whether these models are able to discriminate between El Niño/La Niña years in terms of TC rainfall, and focus on strong El Niño/La Niña events: during JASON of 1997 (El Niño year) and 1998 (La Niña year), and during JFMAM of 1998 and 1999. During JASON 1997 (El Niño developing phase), the TC rainfall in East Asia is suppressed in Japan and Korea and enhanced along the coastal regions of the Bay of Bengal (Fig. 13, top left panel). During the peak seasons of El Niño developing years, fewer TCs make landfall over Japan and Korea than during La Niña years (Zhang et al. 2012, 2016b). Although the La Niña (El Niño) phase is favorable (unfavorable) for TC development in the Bay of Bengal based on observations (Girishkumar and Ravichandran 2012; Felton et al. 2013), the TC rainfall in North India during JASON 1997 is actually associated with a TC making landfall over the eastern coast of India (Fig. 13, top left panel). HiFLOR produces more TC rainfall in Japan, Korea and South China and less in the coastal regions along the Bay of Bengal compared with the observations. In contrast, FLOR underestimates TC rainfall in South

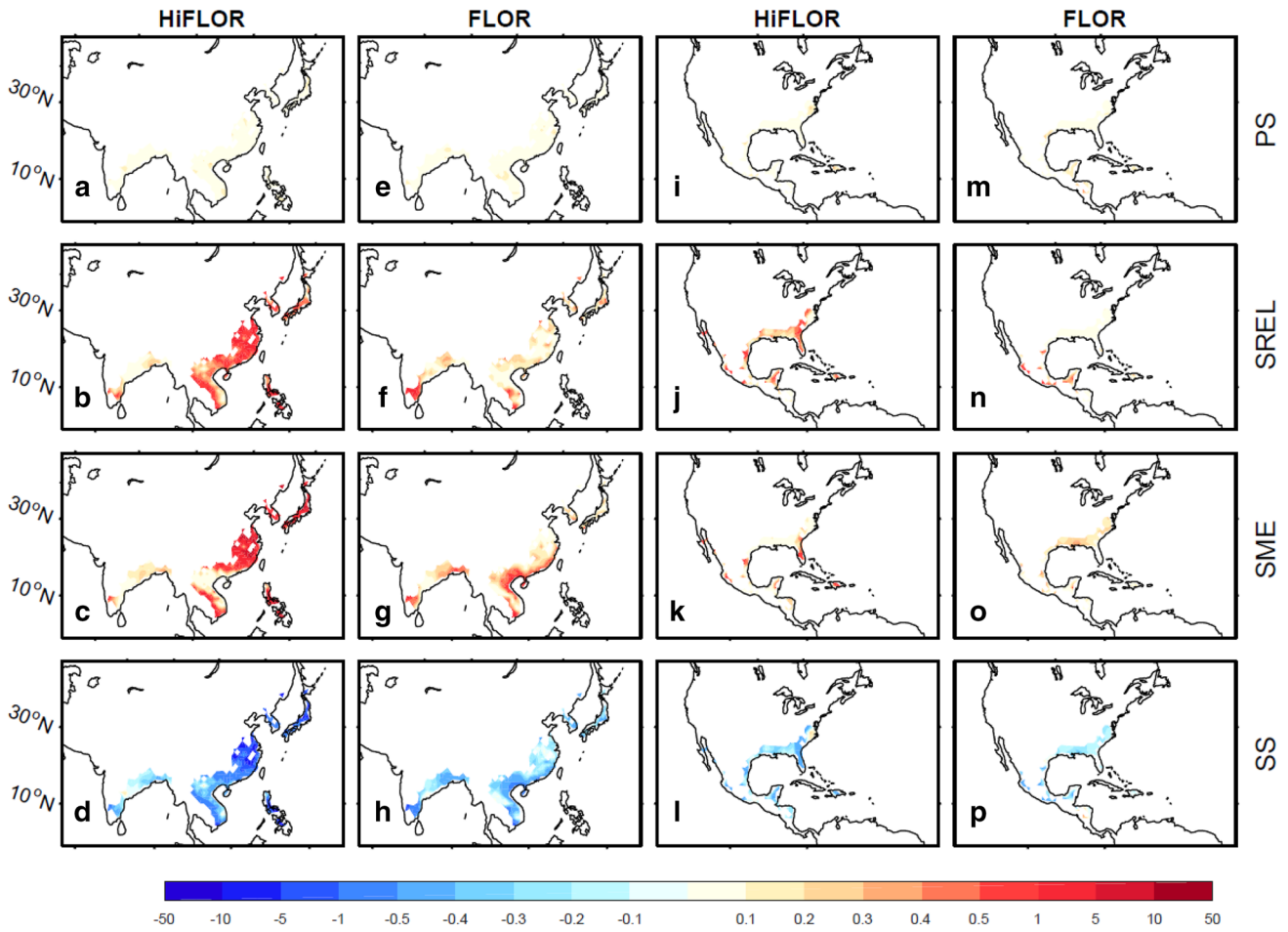

Fig. 9 Maps showing potential skill (**a, e, i, m**), conditional biases (**b, f, j, n**), unconditional biases (**c, g, k, o**), and skill score (**d, h, l, p**) for JASON TC rainfall in Asia and North America using the SST-nudging experiments of HiFLOR and FLOR

China and the coastal regions along the Bay of Bengal, while it overestimates it in Japan and Korea (Fig. 11, bottom left panels).

In JASON 1998 (developing phase of La Niña), TC rainfall is enhanced in Japan, Korea, the Philippines and Thailand, and suppressed in the coastal regions along the Bay of Bengal compared with JASON 1997 (Fig. 13, top right panel). Overall, HiFLOR overestimates the observed TC rainfall while FLOR underestimates the observations (Fig. 13, right panels). In terms of the El Niño–La Niña contrast, HiFLOR captures well the observed differences in TC rainfall between them in Japan, Korea, the Philippines and Thailand, while fails to do so in the coastal regions along the Bay of Bengal (Fig. 13, middle panels). FLOR fails to captures the differences in TC rainfall between El Niño and La Niña in those regions.

In JASON 1997, TC rainfall is suppressed in the United States, while it is enhanced in Central America (Fig. 14, top left panel) because of the reduced TC activity. HiFLOR reproduces the patterns in the observations in North America (Fig. 14, middle left panel), while FLOR underestimates TC rainfall over the regions (Fig. 14, bottom left panel). In JASON 1998, there is enhanced TC activity in the North Atlantic, with larger TC rainfall values in North America than in the previous year; however, compared to the observations and even HiFLOR, these values in FLOR are much smaller and more geographically limited (Fig. 14). Therefore, the results for FLOR indicate that this model is somewhat able to discriminate between different ENSO years; however, the rainfall impacts are much more muted than what we see in the observations. This is not the case when we consider HiFLOR, which is not only able to discriminate

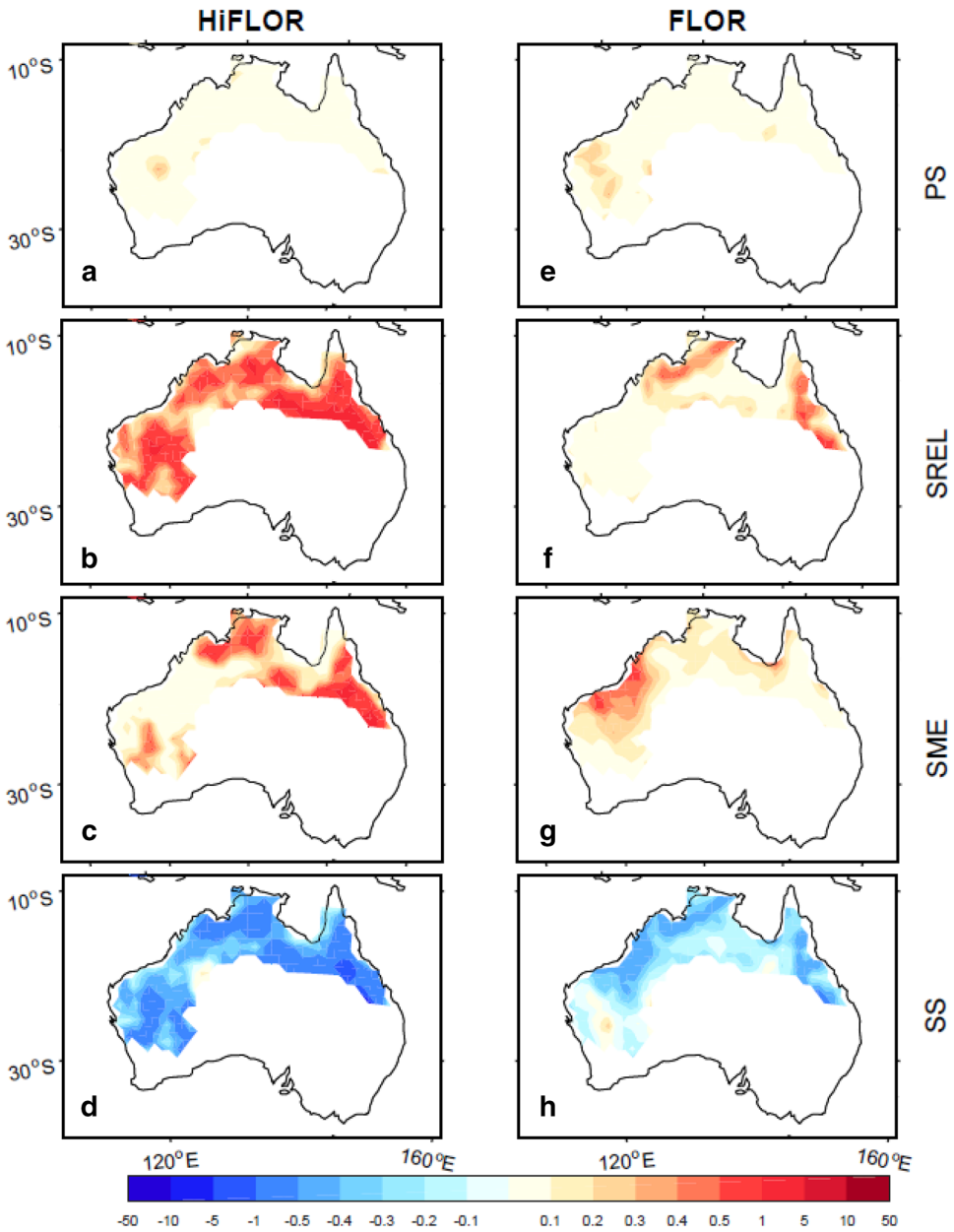

Fig. 10 Maps showing potential skill (**a, e**), conditional biases (**b, f**), unconditional biases (**c, g**), and skill score (**d, h**) for JMFAM TC rainfall in Asia and Australia using the SST-nudging experiments of HiFLOR and FLOR

the TC response for El Niño/ La Niña years, but can also successfully provide information about the associated TC rainfall. While these results are strictly valid for these two models, they point to the improvements in representing the relationship between ENSO and TCs affecting Central and North America using the high-resolution model. However, FLOR seems to outperform HiFLOR in reproducing TC rainfall across much of Central American (e.g., Guatemala, Honduras, El Salvador, and Nicaragua) in JASON 1998 (Fig. 14, left panels).

Australia received little TC rainfall in Western Australia during JFMAM 1998, consistent with the strong El Niño forcing on TC activity in this region (e.g., Kuleshov et al. 2008; Ramsay et al. 2008; Dowdy et al. 2012; Chand et al. 2013). HiFLOR reproduces reasonably well its suppression in Western Australia and TC rainfall in North Australia. However, FLOR dramatically underestimates TC rainfall in northern Australia (Fig. 15, bottom left panel). During JFMAM 1999, there are larger TC rainfall values in western Australia based on observations (Fig. 15, top

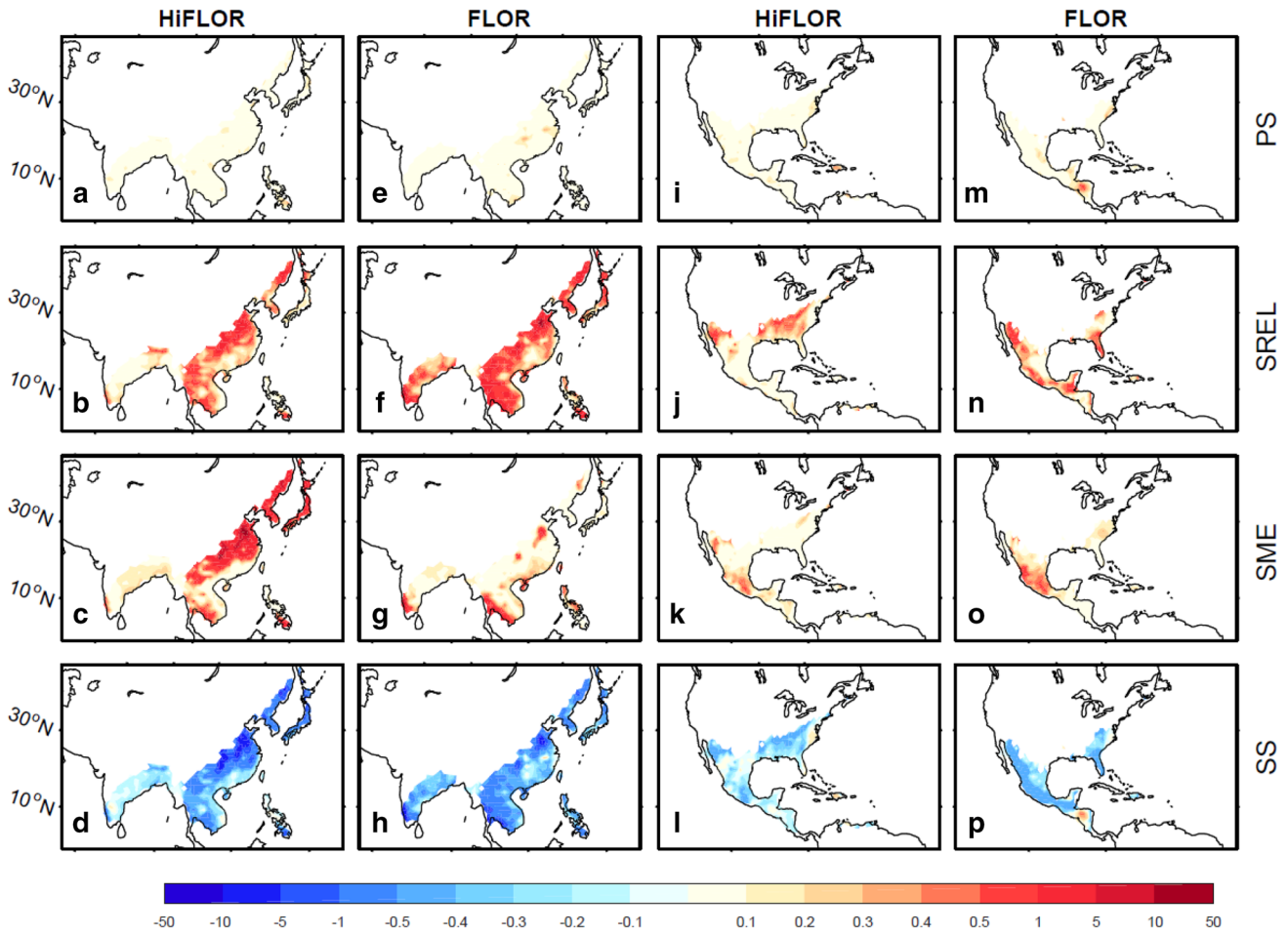

Fig. 11 Maps showing the potential skill (**a, e, i, m**), conditional biases (**b, f, j, n**), unconditional biases (**c, g, k, o**), and skill score (**d, h, l, p**) for proportion of TC rainfall during JASON in Asia and North America using the SST-nudging experiments of HiFLOR and FLOR

right panel), consistent with enhanced TC activity during La Niña phase (e.g., Kuleshov et al. 2008; Chand et al. 2013). HiFLOR reproduces the observed enhanced rainfall in Western Australia during JFMAM 1999, while FLOR's magnitudes are smaller, even though the rainfall footprint is consistent with the observations (Fig. 15, top and bottom right panels). In contrast, HiFLOR overestimates TC rainfall in west and central Australia compared with observations (Fig. 15, top and middle right panels).

4 Discussion and conclusion

While there are multiple hazards associated with TCs, large rainfall amounts are responsible for a large number of fatalities and economic damage. TC rainfall plays therefore a critical role to improve our understanding and preparedness against this hazard. Although many studies have been devoted to the analysis of TC rainfall based on observations, little attention has been paid to climate model simulations and forecast of this quantity with high-resolution TC-permitting GCMs. Here, we have examined the climatology and interannual variability of TC rainfall in the SST-nudging and seasonal-forecast experiments

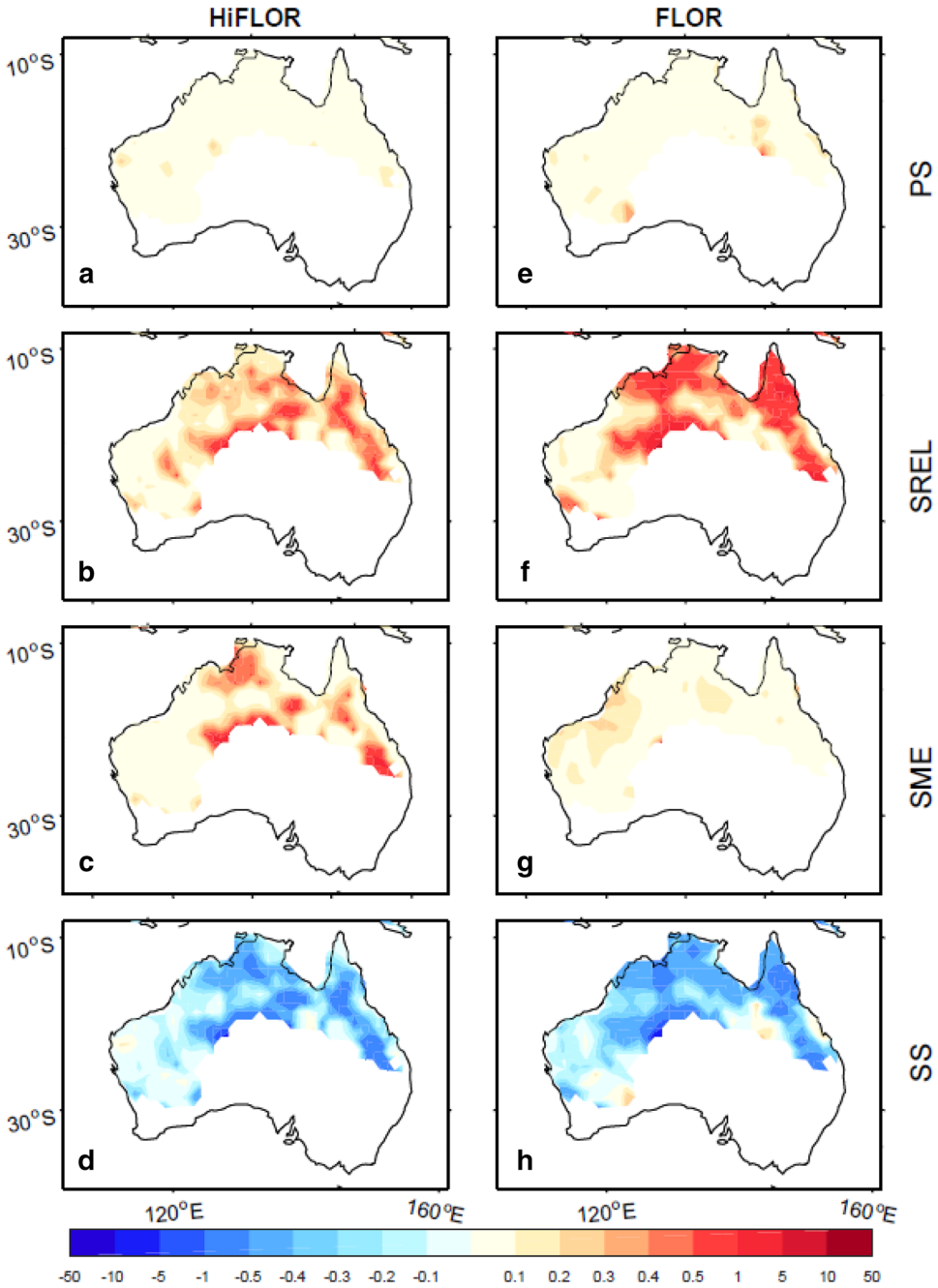

Fig. 12 Maps showing the potential skill (**a, e**), conditional biases (**b, f**), unconditional biases (**c, g**), and skill score (**d, h**) for proportion of TC rainfall during JFMAM in Australia using the SST-nudging experiments of HiFLOR and FLOR

with the TC-permitting HiFLOR and FLOR coupled climate models.

We have examined the year-to-year variation of TC rainfall and its contribution to the seasonal totals in the SST-nudging experiments using HiFLOR and FLOR, and quantitatively evaluated the skill in reproducing the year-to-year variations in TC rainfall. Overall, HiFLOR and FLOR have limited and similar skill in reproducing the interannual variability in these two quantities in Asia, Australia and North America due to the limited potential skill and large conditional and unconditional biases. This suggests that the SST forcing does not reproduce the year-to-year variation in TC rainfall.

Overall, HiFLOR outperforms FLOR in capturing the climatology of TC rainfall during JASON in the SST-nudging and seasonal-forecasting experiments, especially in

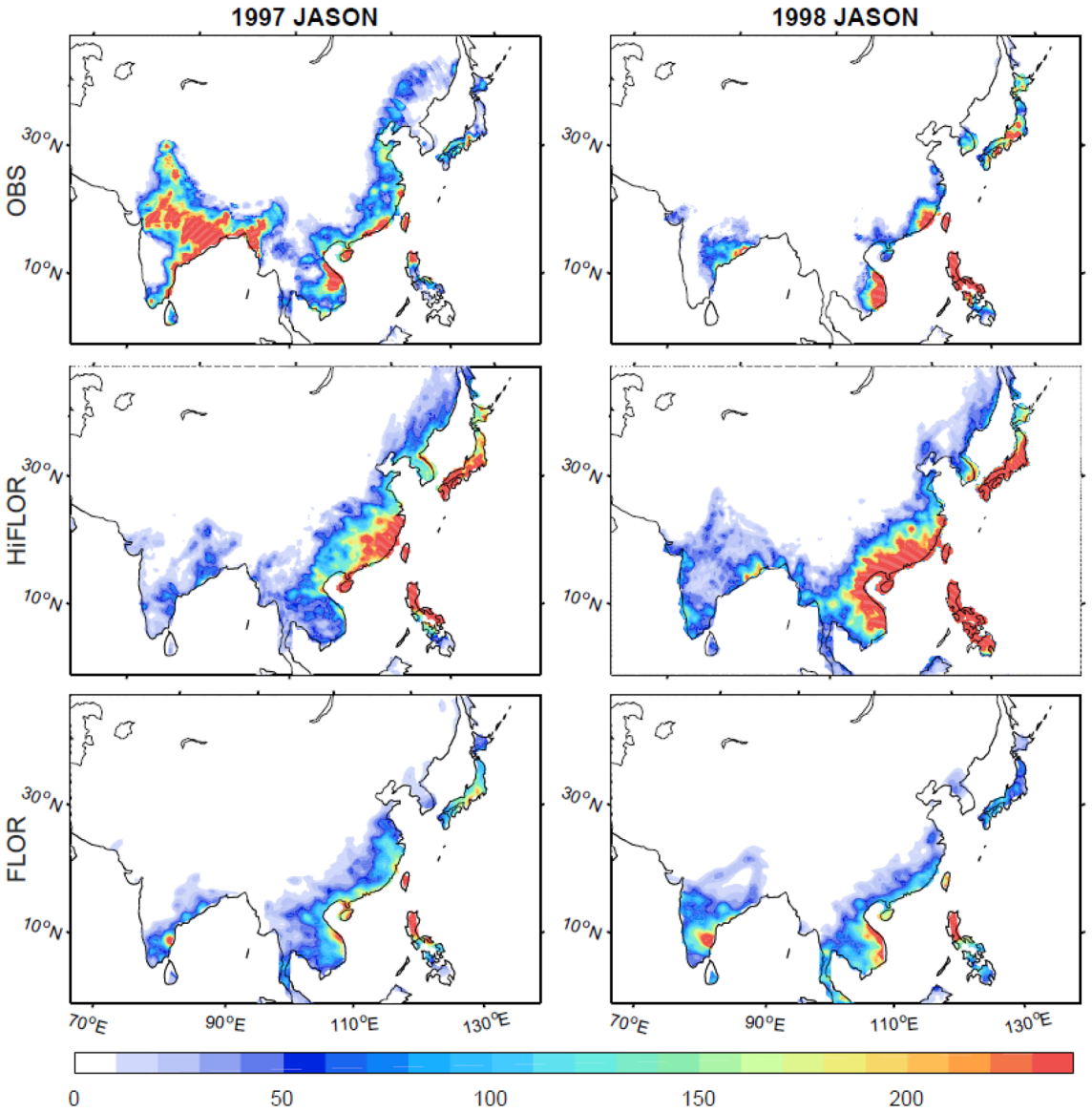

Fig. 13 TC rainfall (unit: mm) in Asia based on (top) the observations, (middle) HiFLOR and (bottom) FLOR during JASON 1997 and 1998

East Asia and North America. During JFMAM, HiFLOR performs much better than FLOR in capturing its climatology of TC rainfall in Australia. However, FLOR tends to produce better results than FLOR during JASON in southeastern India. Both FLOR and HiFLOR underestimate the observed TC rainfall in the coastal regions along the Bay of Bengal during JASON and JFMAM because the two models simulate much lower TC density than observed.

The SST-nudging and seasonal-forecast experiments of FLOR and HiFLOR do not exhibit skill in reproducing the year-to-year variation in TC rainfall due to low potential skill and large biases. This suggests that these two high-resolution GCMs forced by observed SST and radiative forcing cannot reasonably reproduce the interannual variability in the rainfall associated with these storms. This study has focused on TC rainfall over land because most of damages due to TC rainfall occur after the TCs make landfall. The interannual variability of TC rainfall in the seasonal forecasts depends on the interannual variability of TC density. Overall, the forecast skill of TC density over the ocean is much better

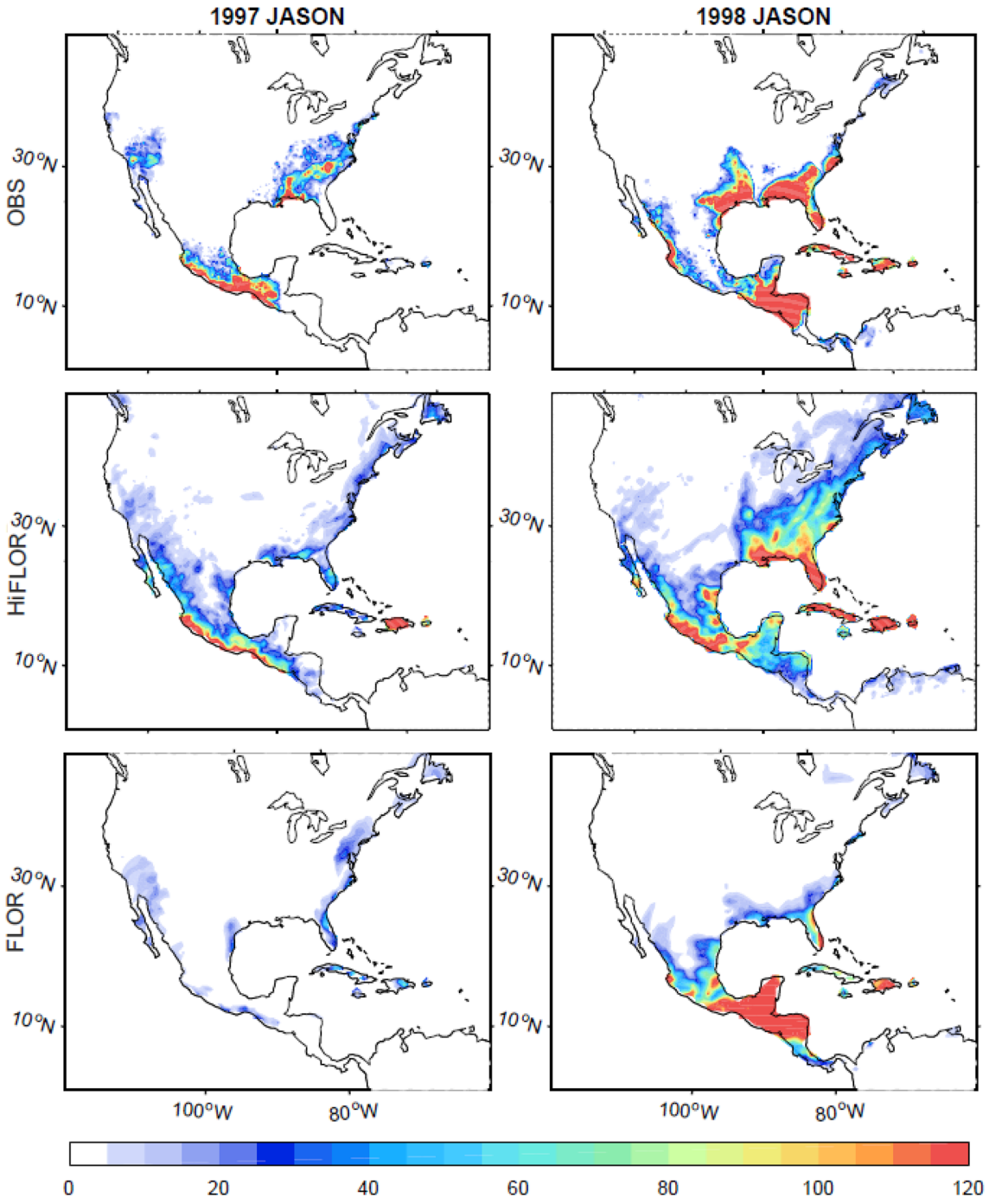

Fig. 14 TC rainfall (unit: mm) in North America based on (top) the observations, (middle) HiFLOR and (bottom) FLOR during JASON 1997 and 1998

than that over the land (Vecchi et al. 2014; Murakami et al. 2016). Therefore, the forecast skill of TC rainfall over the ocean may outperform that over the land.

In interpreting these results, to be able to forecast TC rainfall we need to remember that we would need to correctly forecast their genesis, development and tracking, and then the rainfall distribution around the center of circulation. All these questions are still quite challenging and the subject of research. For example, the shifts in TC genesis locations and tracks are common in climate models (Bell

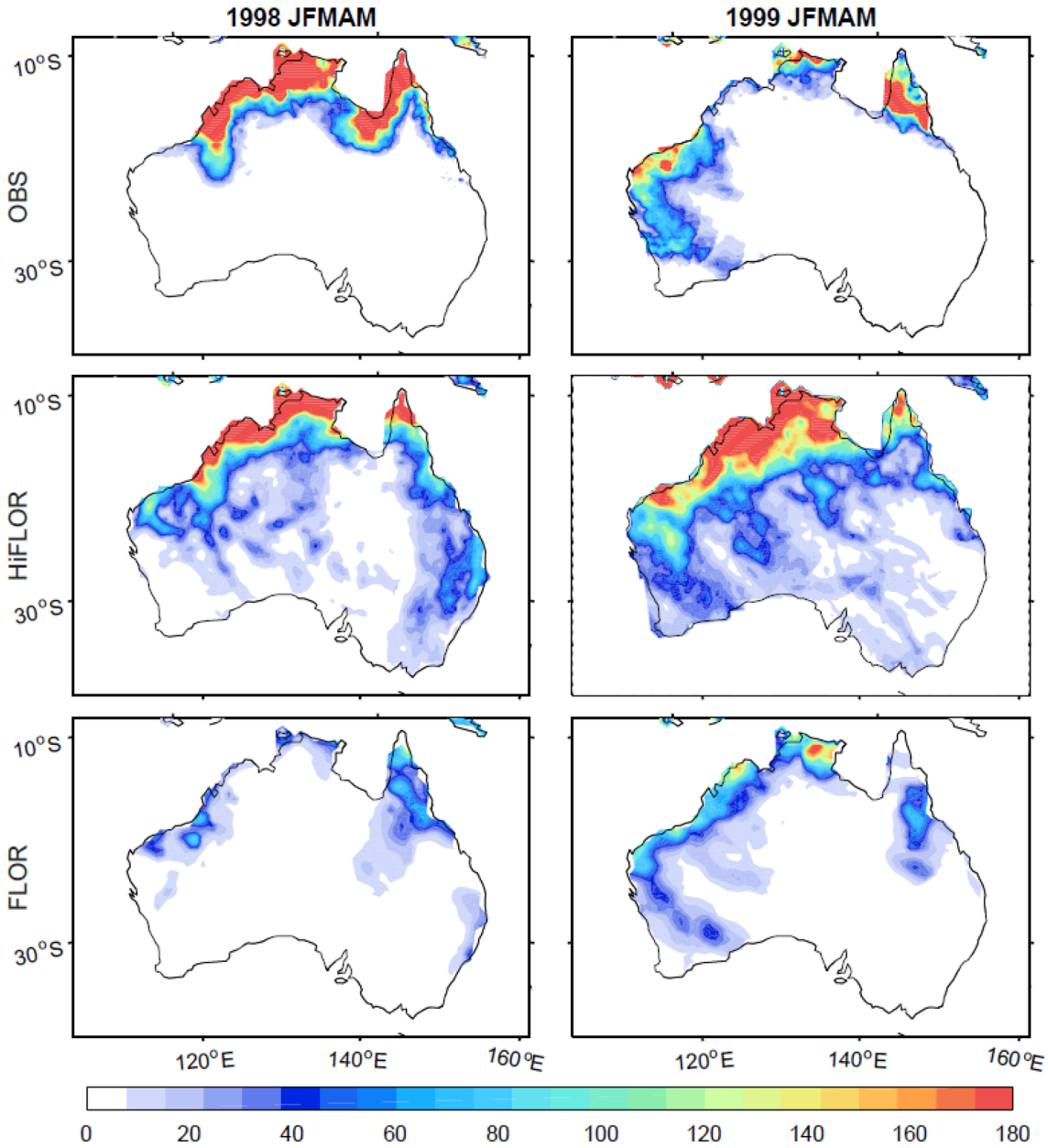

Fig. 15 TC rainfall (unit: mm) in (top) observations, (middle) HiFLOR and (bottom) FLOR during JFMAM of 1998 and 1999

et al. 2014; Shaevitz et al. 2014; Vecchi et al. 2014; Daloz et al. 2015; Camargo and Wing 2016; Murakami et al. 2015, 2016; Zhang et al. 2016b), leading to unrealistic simulations of TC landfall and consequently of the associated rainfall. Recently, HiFLOR appears to simulate the year-to-year variation of landfalling TCs better than FLOR (Murakami et al. 2015, 2016; Zhang et al. 2016b). The future improvements in these aspects of the TC simulations using climate models would lead to improvements in the simulation and seasonal forecasts of year-to-year variation of TC rainfall.

Acknowledgements We are grateful to two anonymous reviewers for helpful comments. This material is based in part upon work supported by the National Science Foundation under Grants AGS-1262091 and AGS-1262099, and Award NA14OAR4830101 from the National Oceanic and Atmospheric Administration, U.S. Department of Commerce.

References

Bagtasa G (2017) Contribution of tropical cyclones to rainfall in the Philippines. J Clim 30:3621–3633

Barlow M (2011) Influence of hurricane-related activity on North American extreme precipitation. Geophys Res Lett 38:L04705

Beck HE, van Dijk AIJM, Levizzani V, Schellekens J, Miralles DG, Martens B, de Roo A (2017a) MSWEP: 3-hourly 0.25° global gridded precipitation (1979–2015) by merging gauge, satellite, and reanalysis data. Hydrol Earth Syst Sci 21:589–615

Beck HE et al (2017b) Global-scale evaluation of 22 precipitation datasets using gauge observations and hydrological modeling. Hydrol Earth Syst Sci 21:6201–6217

Bell R, Hodges K, Vidale PL, Strachan J, Roberts M (2014) Simulation of the global ENSO–tropical cyclone teleconnection by a high-resolution coupled general circulation model. J Clim 27:6404–6422

Camargo SJ, Wing AA (2016) Tropical cyclones in climate models. Wiley Interdiscip Rev Clim Change 7:211–237

Chand SS, Tory KJ, McBride JL, Wheeler MC, Dare RA, Walsh KJ (2013) The different impact of positive-neutral and negative-neutral ENSO regimes on Australian tropical cyclones. J Clim 26:8008–8016

Chen F, Fu Y (2015) Contribution of tropical cyclone rainfall at categories to total precipitation over the Western North Pacific from 1998 to 2007. Sci China Earth Sci 58:2015–2025

Chen Y, Ebert EE, Walsh KJE, Davidson NE (2013) Evaluation of TMPA 3B42 daily precipitation estimates of tropical cyclone rainfall over Australia. J Geophys Res Atmos 118:11966–911978

Czajkowski J, Villarini G, Montgomery M, Michel-Kerjan E, Goska R (2017) Assessing current and future freshwater flood risk from North Atlantic tropical cyclones via insurance claims. Sci Rep 7:41609

Daloz AS et al (2015) Cluster analysis of downscaled and explicitly simulated North Atlantic tropical cyclone tracks. J Clim 28:1333–1361. https://doi.org/10.1175/jcli-d-13-00646.1

Dare RA, Davidson NE, McBride JL (2012) Tropical cyclone contribution to rainfall over Australia. Mon Weather Rev 140:3606–3619

Delworth TL et al (2006) GFDL's CM2 global coupled climate models. Part I: formulation and simulation characteristics. J Clim 19:643–674

Delworth TL et al (2012) Simulated climate and climate change in the GFDL CM2.5 high-resolution coupled climate model. J Clim 25:2755–2781

Dowdy AJ, Qi L, Jones D, Ramsay H, Fawcett R, Kuleshov Y (2012) Tropical cyclone climatology of the South Pacific Ocean and its relationship to El Niño–Southern Oscillation. J Clim 25:6108–6122. https://doi.org/10.1175/jcli-d-11-00647.1

Emanuel K (2017) Assessing the present and future probability of Hurricane Harvey's rainfall. Proc Natl Acad Sci 2017:201716222

Felton CS, Subrahmanyam B, Murty VSN (2013) ENSO-modulated cyclogenesis over the Bay of Bengal. J Clim 26:9806–9818. https://doi.org/10.1175/jcli-d-13-00134.1

Gaona MFR, Villarini G, Zhang W, Vecchi GA (2018) The added value of IMERG in characterizing rainfall in tropical cyclones. Atmos Res 209:95–102. https://doi.org/10.1016/j.atmosres.2018.03.008

Girishkumar MS, Ravichandran M (2012) The influences of ENSO on tropical cyclone activity in the Bay of Bengal during October–December. J Geophys Res Oceans. https://doi.org/10.1029/2011JC007417

Gu X, Zhang Q, Singh VP, Liu L, Shi P (2017) Spatiotemporal patterns of annual and seasonal precipitation extreme distributions across China and potential impact of tropical cyclones. Int J Climatol 37:3949–3962

Harris LM, Lin S-J, Tu C (2016) High-resolution climate simulations using GFDL HiRAM with a stretched global grid. J Clim 29:4293–4314

Hashino T, Bradley AA, Schwartz SS (2007) Evaluation of bias-correction methods for ensemble streamflow volume forecasts. Hydrol Earth Syst Sci 11:939–950

Jiang H, Zipser EJ (2010) Contribution of tropical cyclones to the global precipitation from eight seasons of TRMM data: regional, seasonal, and interannual variations. J Clim 23:1526–1543

Jiang H, Liu C, Zipser EJ (2011) A TRMM-based tropical cyclone cloud and precipitation feature database. J Appl Meteorol Climatol 50:1255–1274

Kam J, Sheffield J, Yuan X, Wood EF (2013) The influence of Atlantic tropical cyclones on drought over the eastern United States (1980–2007). J Clim 26:3067–3086

Kamahori H (2012) Mean features of tropical cyclone precipitation from TRMM/3B42. SOLA 8:017–020. https://doi.org/10.2151/sola.2012-005

Khouakhi A, Villarini G, Vecchi GA (2017) Contribution of tropical cyclones to rainfall at the global scale. J Clim 30:359–372

Knapp KR, Kruk MC, Levinson DH, Diamond HJ, Neumann CJ (2010) The international best track archive for climate stewardship (IBTrACS). Bull Am Meteorol Soc 91:363–376

Knight DB, Davis RE (2009) Contribution of tropical cyclones to extreme rainfall events in the southeastern United States. J Geophys Res Atmos 114:D23102

Knutson TR et al (2010) Tropical cyclones and climate change. Nat Geosci 3:157

Kuleshov Y, Qi L, Fawcett R, Jones D (2008) On tropical cyclone activity in the Southern Hemisphere: trends and the ENSO connection. Geophys Res Lett 35

Langousis A, Veneziano D (2009) Theoretical model of rainfall in tropical cyclones for the assessment of long-term risk. J Geophys Res Atmos 114:D02106

Larson J, Zhou Y, Higgins RW (2005) Characteristics of landfalling tropical cyclones in the United States and Mexico: climatology and interannual variability. J Clim 18:1247–1262

Lau KM, Zhou Y, Wu HT (2008) Have tropical cyclones been feeding more extreme rainfall? J Geophys Res Atmos 113:D23113

Lavender SL, Abbs DJ (2013) Trends in Australian rainfall: contribution of tropical cyclones and closed lows. Clim Dyn 40:317–326

Li Z, Yu W, Li T, Murty VSN, Tangang F (2013) Bimodal character of cyclone climatology in the Bay of Bengal modulated by monsoon seasonal cycle. J Clim 26:1033–1046

Lin Y, Zhao M, Zhang M (2015) Tropical cyclone rainfall area controlled by relative sea surface temperature. Nat Commun 6:6591

Liu M, Vecchi GA, Smith JA, Murakami H (2018) Projection of landfalling–tropical cyclone rainfall in the Eastern United States under anthropogenic warming. J Clim 31:7269–7286

Maxwell JT, Soulé PT, Ortegren JT, Knapp PA (2012) Drought-busting tropical cyclones in the southeastern Atlantic United States: 1950–2008. Ann Assoc Am Geogr 102:259–275

Murakami H et al (2015) Simulation and prediction of category 4 and 5 hurricanes in the high-resolution GFDL HiFLOR coupled climate model. J Clim 28:9058–9079

Murakami H et al (2016) Seasonal forecasts of major hurricanes and landfalling tropical cyclones using a high-resolution GFDL coupled climate model. J Clim 29:7977–7989

Murakami H et al (2017) Dominant role of subtropical pacific warming in extreme Eastern Pacific hurricane seasons: 2015 and the future. J Clim 30:243–264

Murphy AH, Winkler RL (1992) Diagnostic verification of probability forecasts. Int J Forecast 7:435–455. https://doi.org/10.1016/0169-2070(92)90028-8

van Oldenborgh GJ et al (2017) Attribution of extreme rainfall from Hurricane Harvey, August 2017. Environ Res Lett 12:124009

Pascale S et al (2016) The impact of horizontal resolution on North American Monsoon Gulf of California moisture surges in a suite of coupled global climate models. J Clim 29:7911–7936

Pascale S et al (2017) Weakening of the North American monsoon with global warming. Nat Clim Change 7:806

Peterson TC, Hoerling MP, Stott PA, Herring SC (2013) Explaining extreme events of 2012 from a climate perspective. Bull Am Meteorol Soc 94:S1–S74

Prat OP, Nelson BR (2013) Precipitation contribution of tropical cyclones in the southeastern United States from 1998 to 2009 using TRMM satellite data. J Clim 26:1047–1062

Prat OP, Nelson BR (2016) On the link between tropical cyclones and daily rainfall extremes derived from global satellite observations. J Clim 29:6127–6135

Ramsay HA, Leslie LM, Lamb PJ, Richman MB, Leplastrier M (2008) Interannual variability of tropical cyclones in the Australian region: role of large-scale environment. J Clim 21:1083–1103. https://doi.org/10.1175/2007jcli1970.1

Rappaport EN (2014) Fatalities in the United States from Atlantic tropical cyclones: new data and interpretation. Bull Am Meteorol Soc 95:341–346

Risser MD, Wehner MF (2017) Attributable human-induced changes in the likelihood and magnitude of the observed extreme precipitation during hurricane Harvey. Geophys Res Lett 44:12457–412464

Rodgers EB, Adler RF, Pierce HF (2001) Contribution of tropical cyclones to the North Atlantic climatological rainfall as observed from satellites. J Appl Meteorol 40:1785–1800

Rogers R, Marks F, Marchok T (2006) Tropical cyclone rainfall. Encyclopedia of hydrological sciences. Wiley, Oxford

Scoccimarro E, Gualdi S, Villarini G, Vecchi GA, Zhao M, Walsh K, Navarra A (2014) Intense precipitation events associated with landfalling tropical cyclones in response to a warmer climate and increased CO_2. J Clim 27:4642–4654

Scoccimarro E, Villarini G, Gualdi S, Navarra A, Vecchi G, Walsh K, Zhao M (2017) Tropical cyclone rainfall changes in a warmer climate. Hurricanes and climate change. Springer, Berlin, pp 243–255

Shaevitz DA et al (2014) Characteristics of tropical cyclones in high-resolution models in the present climate. J Adv Model Earth Syst 6:1154–1172

Shepherd JM, Grundstein A, Mote TL (2007) Quantifying the contribution of tropical cyclones to extreme rainfall along the coastal southeastern United States. Geophys Res Lett 34:L23810

Skok G, Bacmeister J, Tribbia J (2013) Analysis of tropical cyclone precipitation using an object-based algorithm. J Clim 26:2563–2579

Slater LJ, Villarini G, Bradley AA (2017) Weighting of NMME temperature and precipitation forecasts across Europe. J Hydrol 552:646–659

Vecchi GA et al (2014) On the seasonal forecasting of regional tropical cyclone activity. J Clim 27:7994–8016

Villarini G, Denniston RF (2016) Contribution of tropical cyclones to extreme rainfall in Australia. Int J Climatol 36:1019–1025

Villarini G et al (2014) Sensitivity of tropical cyclone rainfall to idealized global-scale forcings. J Clim 27:4622–4641

Wang C-C, Lin B-X, Chen C-T, Lo S-H (2014) Quantifying the effects of long-term climate change on tropical cyclone rainfall using a cloud-resolving model: examples of two landfall typhoons in Taiwan. J Clim 28:66–85

van der Wiel K et al (2016) The resolution dependence of contiguous U.S. precipitation extremes in response to CO_2 forcing. J Clim 29:7991–8012

Zhang S, Rosati A (2010) An inflated ensemble filter for ocean data assimilation with a biased coupled GCM. Mon Weather Rev 138:3905–3931

Zhang W, Graf H-F, Leung Y, Herzog M (2012) Different El Niño types and tropical cyclone landfall in East Asia. J Clim 25:6510–6523

Zhang W, Vecchi GA, Murakami H, Villarini G, Jia L (2016a) The Pacific meridional mode and the occurrence of tropical cyclones in the Western North Pacific. J Clim 29:381–398

Zhang W et al (2016b) Improved simulation of tropical cyclone responses to ENSO in the Western North Pacific in the high-resolution GFDL HiFLOR coupled climate model. J Clim 29:1391–1415

Zhang W, Villarini G, Vecchi GA (2017) Impacts of the Pacific meridional mode on rainfall over the maritime continent and Australia: potential for seasonal predictions. Clim Dyn 2017:1–15

Zhang W, Vecchi GA, Murakami H, Villarini G, Delworth TL, Yang X, Jia L (2018) Dominant role of atlantic multidecadal oscillation in the recent decadal changes in Western North Pacific tropical cyclone activity. Geophys Res Lett 45:354–362

Zhu L, Frauenfeld OW, Quiring SM (2013) Seasonal tropical cyclone precipitation in Texas: a statistical modeling approach based on a 60 year climatology. J Geophys Res Atmos 118:8842–8856